Figure 1: Structure of section 1. (1) & (2) Along the line of the general prescription developed in section **??**, brane tiling technique realizes the Gauge/YBE correspondence. (3) Brane tiling construction of quiver gauge theories can be rephrased by the language of class-$\mathcal{S}$. (4) A surface defect acting on the index is identified with a transfer matrix acting on the partition function of a corresponding integrable lattice model.

1 Surface defects as transfer matrices

In this section, we mainly review the results in [1], in which the correspondence we introduced in section **??** was established. It turns out that a surface defect is identified with the transfer matrix constructed from the L-operator of Sklyanin or Derkachov-Spiridonov type.

The structure of this section is as follows (see figure 1). (1) We first apply to the brane tilings the general prescription to construct the correspondence between supersymmetric gauge theory and integrable lattice model developed in section **??**. Brane tiling technique allows us to study quiver gauge theories in a systematic way, and taking the four-manifold to be $S^1 \times S^3$, on which quiver gauge theories are defined, the path integral of the twisted partition function of the theory computes the supersymmetric index. (2) For such a case, we will obtain a dictionary between supersymmetric gauge theory and integrable lattice model, which is called *Gauge/YBE correspondence*. (3) The brane tiling construction can be mapped into the setups of the so-called class-$\mathcal{S}$ theories. We proceed to the introduction of surface defects in the simplest case of the theories of class-$\mathcal{S}$. (4) Then we find that the surface defects act on the supersymmetric index by difference operators (1.61) and they are identified with the transfer matrices of the corresponding integrable lattice model (1.62), which is the most important relation of this section:

$$\mathfrak{S}_{(0,1)} = \mathrm{Tr}\left(L^{\diamond}(d,(c,b))\right), \tag{1.1}$$

with an appropriate parameter identification.

1.1 Brane tilings and integrable lattice models

Let us begin with some generalities, before restricting ourselves to the case of $S^1 \times S^3$. In order to give the general argument of the correspondence, we make a brief review of the
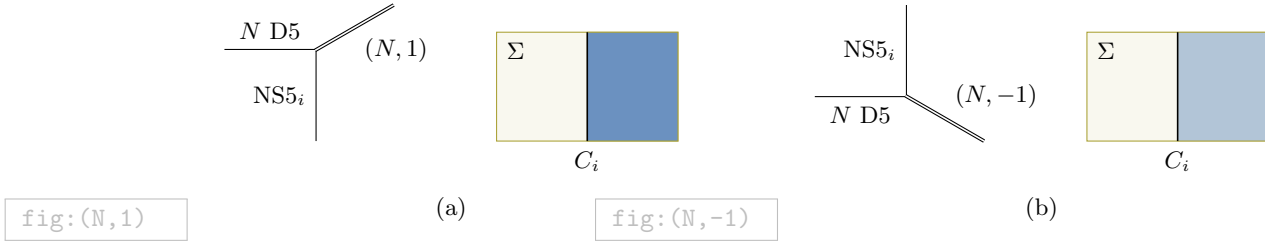
(a)

(b)

Figure 2: An NS5-brane combines with a stack of N D5-branes, forming (a) an $(N, 1)$ 5-brane or (b) an $(N, -1)$ 5-brane. The 5-brane junction is a domain wall in $\mathsf{T}_{\mathrm{D}5}$. The shaded regions shown above support a nonzero NS5-brane charge $q = \pm 1$. In the context of brane tiling, the curves C_i are called zig-zag paths.

systematic brane construction of quiver gauge theories called *brane tilings*. For more details, the reader should be referred to the original papers and the excellent reviews [2–5]. Recall the 5-brane configuration given in section **??**,

$$N \,\mathrm{D}5 \quad S^1 \times M \times \Sigma,$$
$$\mathrm{NS}5_i \quad S^1 \times N_i \times \Sigma_i.$$

For such a configuration, what one needs to notice is that when an NS5-brane meets N D5-branes, they combine to form a bound state. In the language of (p, q) 5-branes, this bound state is either an $(N, 1)$ or $(N, -1)$ 5-brane, depending on the relative positions of the branes; see figure 2. Therefore, the extended defects $\mathcal{E}_{\mathrm{NS}5_i}$ are domain walls in $\mathsf{T}_{\mathrm{D}5}$ separate the spacetime into the regions with different values of the NS5-brane charge q. The curves C_i along which these domain walls are located are known as *zig-zag paths*. Across a zig-zag path the charge q jump by one.

Conversely, given a configuration of curves C_i on the two-dimensional surface Σ and a 5-brane charge assignment consistent with it, we can construct a 5-brane system whose zig-zag paths are C_i: we take NS5-branes approaching the D5-branes from transverse directions, and let them meet along C_i and form bound states over regions with $q \neq 0$. Such a 5-brane system is called a brane tiling on Σ [2, 3].

As we have explained in the last section, a brane tiling gives rise to a four-dimensional $\mathcal{N} = 1$ theory. A concrete description of this theory is known for the subset of brane tilings that involve only $(N, 0)$ 5-branes (i.e. N coincident D5-branes) and $(N, \pm 1)$ 5-branes. Given a brane tiling in this subset, we indicate $(N, 1)$ and $(N, -1)$ 5-brane regions by dark and light shading, respectively, while leaving $(N, 0)$ regions unshaded. After the shading, we get a checkerboard-like pattern on Σ where shaded faces adjoin unshaded ones and two shaded faces sharing a vertex are of different types, see figure 3(a) and 3(c).

Each unshaded region supports N D5-branes, hence an $\mathrm{SU}(N)$ vector multiplet lives there. If the region contains some part of the boundary, the multiplet is frozen by boundary conditions and the associated symmetry is an $\mathrm{SU}(N)$ flavor symmetry; in quiver notation, we represent a dynamical vector multiplet by a gauge node $\bigcirc$ and a non-dynamical one by
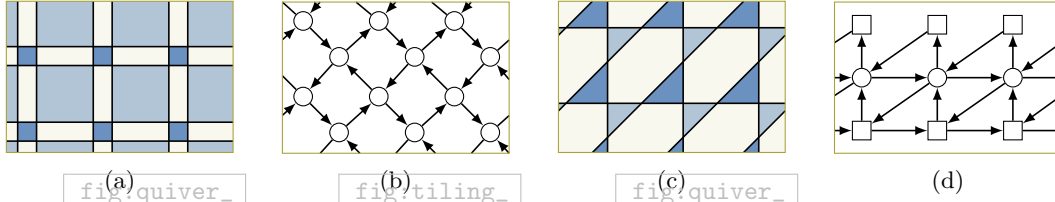
(a) (b) (c) (d)

Figure 3: (a) A brane tiling on a torus. (b) The periodic quiver associated with (a). (c) A brane tiling on a finite-length cylinder. (d) the quiver for (c).

a flavor node $\square$. From open strings stretched between two unshaded regions (namely ending on N D5-branes partitioned by NS5-brane) sharing a vertex, we get a chiral multiplet that transforms in the fundamental representation under one of the associated gauge or flavor groups and in the anti-fundamental representation under the other. We write it by an arrow between the two nodes:

$$ \rightsquigarrow \qquad\qquad (1.2) $$

The arrow points from the anti-fundamental side to the fundamental side. See figure 3 for examples of quivers obtained from brane tilings.

Moreover, for every set of zig-zag paths bounding a shaded region, we have a loop of arrows and world-sheet instantons generate a superpotential term given by the trace of the product of the bifundamental chiral multiplets in the loop. The coefficient of this term is positive or negative depending on whether the direction of the loop is clockwise or counter-clockwise. Thus, the four-dimensional theory realized by a brane tiling in the subset under consideration is an $\mathcal{N} = 1$ supersymmetric gauge theory described by a quiver with potential drawn on Σ.

Each $\mathrm{NS5}_i$ supports a U(1) flavor symmetry $\mathrm{U}(1)_i$. An arrow is charged under $\mathrm{U}(1)_i$ if it is crossed by C_i. The charge F_i of $\mathrm{U}(1)_i$ can be normalized in such a way that the arrow in (1.2) has $F_i = -1$ and $F_j = +1$. The diagonal combination of all $\mathrm{U}(1)_i$ acts on the theory trivially since every arrow is crossed by exactly two zig-zag paths from the opposite sides.

The theory also has an R-symmetry $\mathrm{U}(1)_R$. Its definition is not unique as the R-charge R can be shifted by a linear combination of U(1) flavor charges. However, the R-charge assignment is constrained by two conditions. The first is that $\mathrm{U}(1)_R$ must be unbroken by the superpotential and therefore the R-charges of the chiral multiplets contained in each superpotential term must add up to two. The second is that $\mathrm{U}(1)_R$ must be anomaly free. This requires that for every gauge node, the sum of the R-charges of the arrows starting from or ending at that node must equal the number of the arrows minus two.

To fix the R-charge assignment, let us assume that we can orient the zig-zag paths and bound every shaded or unshaded region with zig-zag paths all heading upward, for some choice of the "vertical" direction in the neighborhood of that region. This is the case for
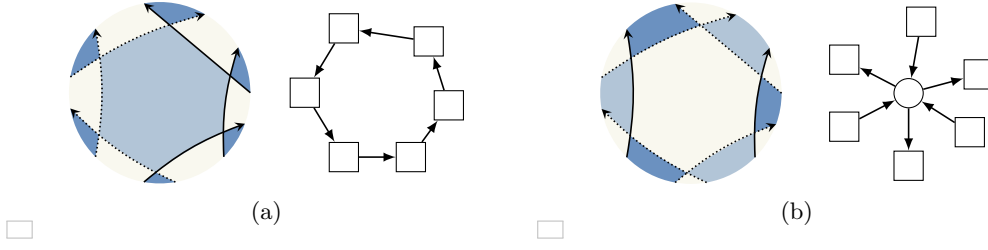
Figure 4: Zig-zag paths bounding (a) a shaded region and (b) an unshaded region. In either case, the R-charges of two of the arrows are different from those of the rest.
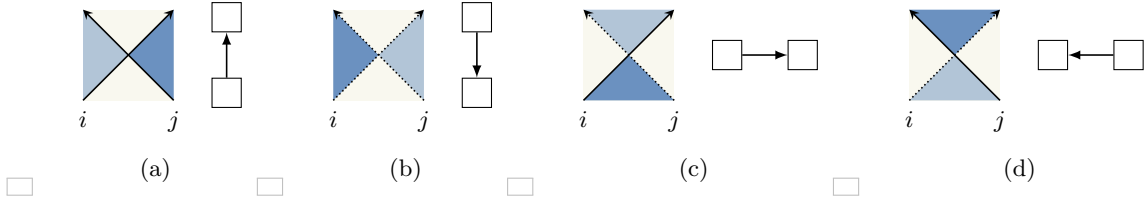
Figure 5: The rule for assigning a quiver to a brane tiling diagram. The arrows in (a) and (b) have $(R, F_i, F_j) = (0, -1, 1)$. Those in (c) and (d) have $(R, F_i, F_j) = (1, 1, -1)$.

the examples in figure 3. The zig-zag paths are thus oriented and fall into two groups; when a zig-zag path goes upward and we cross it from the left to the right, q increases by one. We distinguish the latter case from the former by drawing the zig-zag path with a dotted line. Then, we give an arrow $R = 0$ if it originates from a crossing of two zig-zag paths of the same type, and $R = 1$ otherwise. With this R-charge assignment the two conditions described above are satisfied; see figure 4.

Summarizing the rules for assignment of the charges, we can read off the quiver diagram from zig-zag paths as in figure 5.

1.1.1 Integrable lattice models from quiver gauge theories

From the supersymmetric index of the four-dimensional $\mathcal{N} = 1$ theory realized by a brane tiling, we obtain an integrable lattice model defined on the lattice $\{C_i\}$ consisting of the zig-zag paths. Each C_i carries a spectral parameter u_i. S-duality followed by T-duality on S^1 turns $\mathrm{NS5}_i$ into a D4-brane, and its coordinate on the dual circle $\tilde{S}^1$ is u_i. Instead, we can apply T-duality on S^1 and lift $\mathrm{NS5}_i$ to an M5-brane, then u_i becomes the coordinate on the M-theory circle. Either way, u_i is determined by the holonomy of the U(1) gauge field on $\mathrm{NS5}_i$ along S^1.

If the theory is described by a quiver diagram, translation between gauge theory and lattice model goes as follows [6,7]. Nodes in the quiver diagram are interpreted as spin sites. For each flavor node, we can turn on a holonomy of the associated gauge field. The index depends on the conjugacy class of the holonomy, which is uniquely represented by a diagonal matrix $\mathrm{diag}(z_1, \ldots, z_N)$ up to permutations of the entries. The index is therefore a symmetric

function of the U(1)-valued variables $(z_1, \ldots, z_N)$ obeying the constraint $z_1 \cdots z_N = 1$. These variables are fugacities for the $SU(N)$ flavor symmetry and parametrize the value of the spin at this node, and thus the spins take values in the maximal torus $U(1)^{N-1}$ of $SU(N)$. For a gauge node, integration is performed over the fugacities since its gauge field is a path integral variable. This is the summation over the values of a spin placed on an internal face. Finally, arrows in the quiver diagram represent interactions between spins. In view of quivers, the interaction between spins may chiral in many cases.
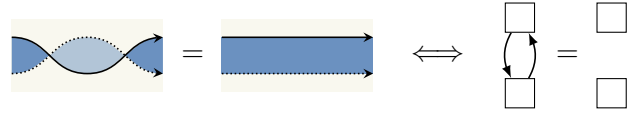
The unitarity relations in lattice model side are satisfied if the contributions to the index from arrows with $R = 0$ are properly normalized. For example, consider the relation[1]

$$\tag{1.3}$$

where the right-hand side is a "delta function" that equates two flavor nodes when one of them is gauged. The theory on the left-hand side is SQCD with N colors and N flavors. It exhibits confinement and has a vacuum in which the mesons take nonzero expectation values and the flavor symmetry $SU(N) \times SU(N)$ is broken to the diagonal subgroup [8]. The index computed in this vacuum is given by the right-hand side, provided that we cancel the contributions from the surviving baryon and anti-baryon. Another unitarity relation

$$\tag{1.4}$$
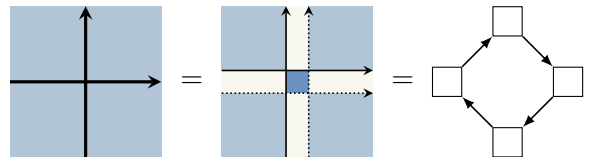
holds since the two arrows on the left-hand side form a loop and generates a mass term in the superpotential. We can send the mass to infinity so that these arrows decouple from the theory, and are left with the right-hand side. We will come back to these points at the explicit computation of the index.

The Yang-Baxter equation with three zig-zag paths is harder to understand, as it always involves (N, q) region with $|q| > 1$ and a quiver description is not available. The problem stems from the fact that our defects are domain walls across which q changes. To circumvent the difficulty, we take a pair of zig-zag paths of different types and think of it as a single line:

$$\tag{1.5}$$

This line does not alter the value of q. Taking two copies of this line and placing them in an $(N, -1)$ background, we can make the R-matrix

$$\tag{1.6}$$

---

[1]By an equality of two quiver diagrams, we mean that the supersymmetric indices of the theories described those quivers are equal. The precise meaning will be given for the $S^1 \times S^3$ case below.

A lattice model constructed from this R-matrix is a vertex model whose quiver consists of diamonds of arrows; see figure 3(b). The vector space carried by a line is the space of symmetric functions of fugacities $(z_1, \ldots, z_N)$.

Alternatively, we can place these lines in an $(N, 0)$ background and force them to exchange their constituent zig-zag paths as they cross:

$$
\tag{1.7}
$$

This R-matrix leads to an IRF model described by a quiver with triangles of arrows, as shown in figure 3(d). The corresponding Yang-Baxter equation, after cancellation of some factors with the help of the unitarity relation (1.3), reads

$$
\tag{1.8}
$$

The two sides are related by Seiberg duality [9] for SQCD with N colors and $2N$ flavors, so their indices are indeed equal. The Yang-Baxter equation in the lattice model in this case is hence also identified with the Seiberg duality in gauge theory side. The relation between the Yang-Baxter move and Seiberg duality was first pointed out in [10] and established in [6]. The Yang-Baxter equation for the R-matrix (1.6), which will be our main focus though more complicated, also follows from this equality.

1.1.2 Supersymmetric index on $S^1 \times S^3$ and Gauge/YBE correspondence

Let us be more specific. Based on the observations so far, here we demonstrate that for the case of $M = S^3$, namely given the four-manifold $S^1 \times S^3$, the supersymmtric index indeed matches the partition function of an integrable lattice model. Furthermore, in this case the correspondence between supersymmetric gauge theory and integrable lattice model has a clear one-by-one dictionary, as we will see.

We now focus on the case $M = S^3$, in which geometry the supersymmetric index is well-studied from the works by [11–13]. Parametrize S^3 by two complex variables (ζ_p, ζ_q) satisfying $|\zeta_p|^2 + |\zeta_q|^2 = 1$, and denote the isometry groups acting on ζ_p and ζ_q by $U(1)_p$ and $U(1)_q$, respectively. We take $S^1 \times S^3$ to be a twisted product; we prepare a trivial S^3-fibration over an interval $[0, \beta]$ and identify the fibers at the ends of the base using an isometry $\left(e^{i\theta_p}, e^{i\theta_q} \right) \in U(1)_p \times U(1)_q$. On this spacetime, the partition function of the quiver gauge theory realized by a brane tiling gives the supersymmetric index refined by the isometries and the flavor symmetries.

The index is defined as a trace of refined Boltzmann weight over the space of states on S^3, which is computed exactly using state-operator correspondence in conformal case or by localization of the path integral. For $\mathcal{N} = 1$ quiver gauge theories on $S^1 \times S^3$, it is

$$\mathcal{I}(p, q, \{a_i\}) = \text{Tr}_{\mathcal{H}_{S^3}} \left((-1)^F p^{j_1 + j_2 + R/2} q^{j_1 - j_2 + R/2} \prod_i a_i^{F_i} \right), \tag{1.9}$$

where the trace is taken over the space $\mathcal{H}_{S^3}$ of states on S^3. Here $(-1)^F$ is the fermion parity, and j_1, j_2 are generators of the maximal torus $\text{U}(1)_1 \times \text{U}(1)_2$ of the isometry group $\text{Spin}(4) \simeq \text{SU}(2)_1 \times \text{SU}(2)_2$ of S^3, $\{a_i\}$ and p, q are complex parameters.

Building blocks of four-dimensional $\mathcal{N} = 1$ supersymmetric quiver gauge theories are vector multiplets and bifundamental chiral multiplets. A vector multiplet is present at a gauge node. A bifundamental chiral multiplet has two flavor groups, say $\text{SU}(N)_z$ and $\text{SU}(N)_w$.[2] The full index is generically given by a combination of vector and chiral multiplets involved in the theory. These multiplets are expressed in terms of the elliptic gamma function

$$\Gamma(z; p, q) = \prod_{j,k=0}^{\infty} \frac{1 - p^{j+1} q^{k+1} z^{-1}}{1 - p^j q^k z}. \tag{1.10}$$

To write down the index, let $a_i = e^{2\pi i u_i}$ be the fugacity for the flavor group $\text{U}(1)_i$ associated with the ith zig-zag path. Also, we use the Pochhammer symble $(z; q)_\infty = \prod_{k=0}^{\infty} \left(1 - q^k z \right)$. For useful formulas for the elliptic gamma function and relations with theta functions, see appendix **??**.

Given a theory $\mathcal{T}$ with flavor group $\text{SU}(N)_w$ and another theory $\mathcal{T}'$ with flavor group $\text{SU}(N)_{w'}$, we can couple them to obtain a new theory $(\mathcal{T} \times \mathcal{T}') / \text{SU}(N)_z$ by gauging the diagonal subgroup $\text{SU}(N)_z$ of $\text{SU}(N)_w \times \text{SU}(N)_{w'}$. To construct a quiver gauge theory, we take a number of bifundamental chiral multiplets and couple them by gauging all or part of the flavor nodes.

The index $\mathcal{I}_\mathcal{T}$ of a four-dimensional $\mathcal{N} = 1$ theory $\mathcal{T}$ with flavor group $\text{SU}(N)_z$ is a symmetric meromorphic function of the fugacities $z_1, \ldots, z_N$. This symmetric property reflects the gauge invariance of the index. At the level of the index, gauging of a flavor group is realized by introducing the corresponding vector multiplet and integration over its fugacities. For example,

$$\mathcal{I}_{(\mathcal{T} \times \mathcal{T}') / \text{SU}(N)_z} = \int_{\mathbb{T}^{N-1}} \prod_{I=1}^{N-1} \frac{dz_I}{2\pi i z_I} \mathcal{I}_V(z) \mathcal{I}_\mathcal{T}(z) \mathcal{I}_{\mathcal{T}'}(z), \tag{1.11}$$

with the integration performed over the unit circle $\mathbb{T}$ for each variable z_I. The index $\mathcal{I}_\mathcal{T}(z)$ of the vector multiplet is given by elliptic gamma functions:

$$\boxed{z} = \mathcal{I}_V(z; p, q) = \frac{(p; p)_\infty^{N-1} (q; q)_\infty^{N-1}}{N!} \prod_{\substack{I,J=1 \\ I \neq J}}^{N} \frac{1}{\Gamma(z_I / z_J; p, q)}. \tag{1.12}$$

---

[2]We label gauge and flavor groups by their associated fugacities, say z. The same applies to the nodes appearing below, since the rank of them is fixed.

Here and in the following, we are often using a quiver to mean the index of the corresponding theory. From now on we fix p, q and omit them from the notation unless needed.

The index of a bifundamental chiral multiplet with fugacity a is given by

$$\boxed{z}\xrightarrow{a}\boxed{w} = \mathcal{I}_B(z,w;a) = \prod_{I,J=1}^{N} \Gamma\left(a\frac{w_I}{z_J}\right). \tag{1.13}$$

This function satisfies

$$\mathcal{I}_B(z,w;a)\mathcal{I}_B\left(w,z;\frac{pq}{a}\right) = 1. \tag{1.14}$$

This identity corresponds the unitarity relation (1.4) and says that as far as the index is concerned, we can cancel a pair of arrows making a loop if their R-charges add up to 2 and flavor charges add up to 0:

$$\boxed{z}\overset{a}{\underset{pq/a}{\rightleftarrows}}\boxed{w} = \boxed{z} \qquad \boxed{w} \;. \tag{1.15}$$

Physically, the reason is again that we can turn on mass term for such a pair. The index is invariant under this deformation, and the bifundamental chiral multiplets decouple from the theory if we send the mass to infinity, leaving a trivial contribution to the index. We will make use of this identity frequently.

Another useful fact is that if we define the "delta function"

$$\boxed{z}=\!\!=\!\!=\boxed{w} \tag{1.16}$$

by the relation

$$\mathcal{I}_\mathcal{T}(w) = \int_{\mathbb{T}^{N-1}} \prod_{I=1}^{N-1} \frac{dz_I}{2\pi i z_I} \mathcal{I}_V(z)\mathcal{I}_\mathcal{T}(z)\boxed{z}=\!\!=\!\!=\boxed{w}\,, \tag{1.17}$$

then we have

$$\boxed{z}\xrightarrow{a}\underset{}{\textcircled{x}}\xrightarrow{a^{-1}}\boxed{w} = \int_{\mathbb{T}^{N-1}} \prod_{I=1}^{N-1} \frac{dx_I}{2\pi i x_I} \mathcal{I}_V(x)\mathcal{I}_B(z,x;a)\mathcal{I}_B\left(x,w;a^{-1}\right)$$
$$= \Gamma\left(a^{\pm N}\right)\boxed{z}=\!\!=\!\!=\boxed{w}\;. \tag{1.18}$$

This corresponds to the other unitarity relation (1.3) and implies a consequence of confinement and chiral symmetry breaking [8,14]. The theory on the left-hand side has a vacuum in which the mesons take nonzero expectation values and the flavor symmetry $\mathrm{SU}(N)_w\times\mathrm{SU}(N)_z$ is broken to the diagonal subgroup. In this vacuum the fugacities w and z are identified, so we get the quiver on the second line. The $\Gamma(a^{\pm N}) := \Gamma(a^N)\Gamma(a^{-N})$ is the contribution from the baryons, and so the unitarity relation (1.3) is satisfied if we normalize the contribution from each arrow with $R = 0$ by dividing it by this factor. The Yang-Baxter equation (1.8) is an integral identity obeyed by the elliptic gamma function [15–17].

We can readily write down the formula for the full index of a general quiver gauge theory. For simplicity, suppose that the theory is described by a quiver that contains no flavor node.
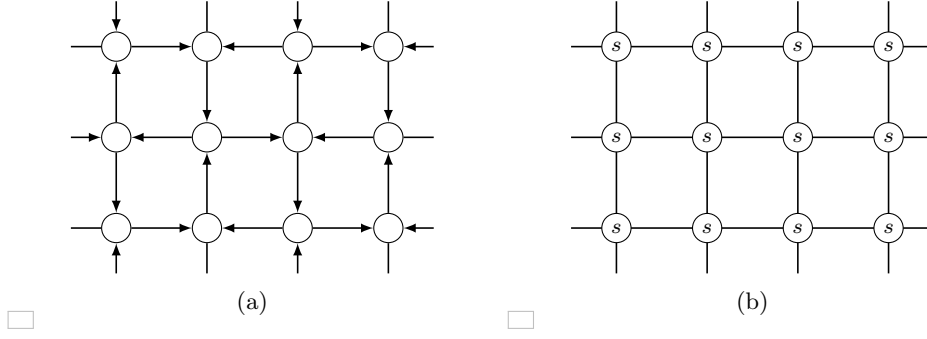
(a)   (b)

Figure 6: (a) A quiver diagram specifying a gauge theory. On each node and each edge, vector multiplet and bifundamental chiral multiplet contribute to the index. (b) A spin system associated with the quiver diagram (a), defined on the same lattice. Spins and their interaction specify a lattice model. The nearest-neighbor interaction may be chiral.

Then, the index is computed by

$$\prod_{\textcircled{z}} \int_{\mathbb{T}^{N-1}} \prod_{I=1}^{N-1} \frac{dz_I}{2\pi i z_I} \mathcal{I}_V(z) \prod_{\textcircled{x} \rightarrow \textcircled{y}} \mathcal{I}_B(x,y), \tag{1.19}$$

where the two products are taken over all nodes and all arrows, respectively. the index is a function of the parameters p, q and the flavor fugacities a_i, which are suppressed in the above expression. If the quiver contains flavor nodes, the index is also a function of their fugacities.

In the expression of the full index (1.19), it is manifest that the index of a quiver gauge theory may be interpreted as the partition function of a statistical mechanical model with continuous spins. Indeed, this formula precisely computes the partition function of a spin model in which spins are placed at gauge nodes [6,18]. The spin variables at the gauge nodes are the fugacities $z_1, \ldots, z_N$, and they interact among themselves as well as with spins at nearest-neighbor nodes, namely those connected by arrows. The Boltzmann weights for the self-interaction and the nearest-neighbor interaction are given by $\mathcal{I}_V$ and $\mathcal{I}_B$, respectively; see figure 6. Integration over fugacities is a counterpart of the summation over all the allowed spin configurations in lattice model side. What is more, the quantities in four-dimensional gauge theories really have one-to-one correspondence in the lattice model side. The dictionary is shown as in table 1 and such a correspondence is called *Gauge/YBE correspondence*.

1.2   Class-$\mathcal{S}$ theories in brane tilings

In section 1.3, we introduce surface defects in theories of class-$\mathcal{S}$ and compare them with transfer matrices of an integrable lattice model. As a preparation, here we review some basic facts of class-$\mathcal{S}$ theory and make a map from the brane tiling setups considered above to the class-$\mathcal{S}$ language.

9

Table 1: Dictionary for the Gauge/YBE correspondence

Integrable lattice model	Quiver gauge theory
Spin lattice	Quiver diagram
Spin variables	Maximal torus (Cartan subalgebra) of gauge group
Self-interaction	Vector multiplet
Nearest-neighbor interaction	Bifundamental matter multiplet
Statistical partition function	Supersymmetric index
Number of spin components	Rank of gauge group
Temperature-like parameters	Quantum parameters (such as p, q)
Rapidity line	Zig-zag path
Spectral parameter	Holonomy of U(1) gauge field
R-matrix	Index for the corresponding quivers
Yang-Baxter equation	Seiberg(-like) duality
Composition of R-matrices	Gauging

Table 2: D4-NS5 brane configuration

	0	1	2	3	4	5	6	7	8	9
D4	×	×	×	×			×			
NS5	×	×	×	×	×	×				

1.2.1 $\mathcal{N} = 2$ quiver theories from class-$\mathcal{S}$

The theories of class-$\mathcal{S}$ is first suggested by Gaiotto [19], and established in [20]. Such theories arise from compactification of six-dimensional $\mathcal{N} = (2,0)$ superconformal field theory, or M5-brane, on punctured Riemann surfaces. The idea of class-$\mathcal{S}$ leads to various correspondences among QFTs in diverse dimensions, including the renowned AGT correspondence [21, 22] and the variants thereof [23–29].

Typical examples of class-$\mathcal{S}$ theories are $\mathcal{N} = 2$ gauge theories characterized by linear and circular quivers with SU(N) nodes. They are actually also examples of brane tiling models discussed in the previous sections. As such, they allow us to translate key notions in class-$\mathcal{S}$ theories to the language of brane tilings, and vice versa. So let us first describe these theories as class-$\mathcal{S}$ theories as well as brane tiling models, and understand the relation between the two descriptions. Although we will mainly work with $N = 2$, for now we keep N general.

Let us consider the standard type IIA brane configuration for an $\mathcal{N} = 2$ linear quiver theory with $m + 1$ nodes. It consists of N D4-branes spanning the 01236 directions, intersected by m NS5-branes extending along the 012345 directions; see table 2. This brane configuration is lifted in M-theory to M5-branes, wrapped on a cylinder with m punctures created by intersecting M5-branes. Therefore, the $\mathcal{N} = 2$ linear quiver theory is obtained by
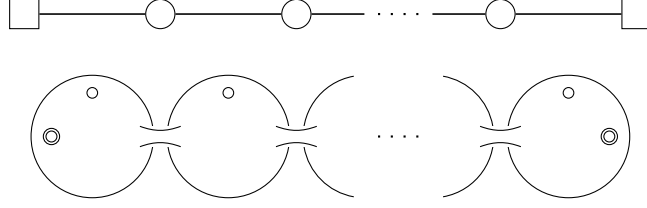
Figure 7: An $\mathcal{N} = 2$ linear quiver theory associated to a punctured sphere.

compactification of the six-dimensional $\mathcal{N} = (2,0)$ theory of type A_{N-1} on a cylinder with m punctures, or a sphere with $m + 2$ punctures. We distinguish the two punctures coming from the ends of the cylinder from the m punctures in between. They are referred to as maximal and minimal punctures, respectively. In the class-$\mathcal{S}$ language, the $\mathcal{N} = 2$ linear quiver theory is a theory associated to a sphere with 2 maximal and m minimal punctures; see figure 7.

R-symmetry of the theory is $\mathrm{SU}(2)_I \times \mathrm{U}(1)_r$, where $\mathrm{SU}(2)_I$ represents the rotation symmetry of the 789-space, and $\mathrm{U}(1)_r$ the rotation symmetry of the 45-plane. The $\mathrm{SU}(N)$ flavor node from each end of the quiver is associated to the maximal puncture on the corresponding side of the sphere. The ith gauge node is associated to the tube between the ith and $(i+1)$th minimal punctures. To the ith minimal puncture is associated a flavor symmetry $\mathrm{U}(1)_i$ which acts on the hypermultiplet charged under the $(i-1)$th and ith gauge nodes.

Following the philosophy of class-$\mathcal{S}$ theories, we decompose this theory into basic building blocks by decoupling gauge fields. Roughly, the gauge coupling of the ith gauge node is inversely proportional to the length between the ith and $(i+1)$th minimal punctures. To make the gauge couplings small, we take the minimal punctures far apart from one another. Then the surface looks like a string of m spheres, each containing a single minimal puncture, connected by long tubes. The smaller the gauge couplings get, the longer the tubes become, and eventually these spheres split up as the couplings go to zero. Each of the spheres represents a bifundamental hypermultiplet, which is a linear quiver with $m = 1$, so it has one minimal and two maximal punctures. The quiver thus breaks into a collection of three-punctured spheres, or trinions.

Conversely, a sphere with two maximal and m minimal punctures is obtained by gluing m trinions together by replacing pairs of maximal punctures with tubes. In general, we can connect two Riemann surfaces with a tube at maximal punctures. From the gauge theory point of view, gluing corresponds to gauging the diagonal combination of the $\mathrm{SU}(N)$ flavor symmetries associated to the maximal punctures involved. Using trinions with one minimal and two maximal punctures, we can obtain any linear quiver in this way, and for that manner also a circular quiver by further gluing the two ends of a linear quiver together. In this sense, these trinions are building blocks for linear and circular quivers. As these two kinds of quivers can be treated essentially in the same manner, we will focus on linear quivers in the followings.
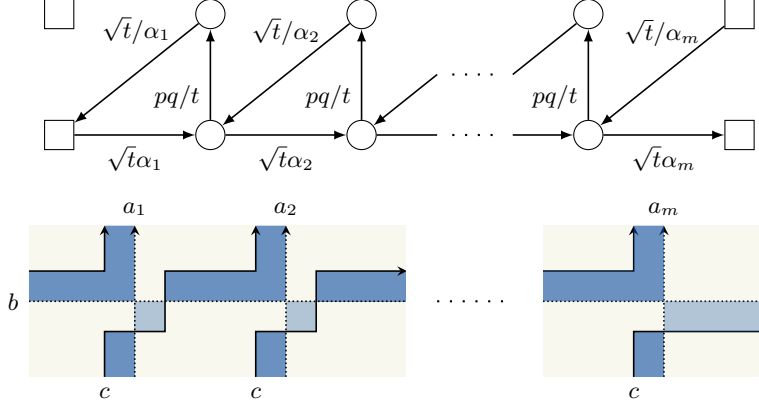
Figure 8: An $\mathcal{N} = 2$ linear quiver as a brane tiling model. In the quiver, the two nodes in the same column are identified and it reproduces the quiver in figure 7. In the brane tiling diagram, the vertical direction is periodic.

1.2.2 Class-$\mathcal{S}$ theories from brane tiling

To make contact with brane tilings, what we need to do is to find the counterpart of trinion, building block of quiver gauge theories, in brane tiling systems. To do this, we describe the $\mathcal{N} = 2$ linear quiver theory as an $\mathcal{N} = 1$ quiver gauge theory. In terms of $\mathcal{N} = 1$ supermultiplets, the $\mathcal{N} = 2$ vector multiplet for the ith gauge node decomposes into a vector multiplet and a chiral multiplet Φ_i in the adjoint representation with $(r, I_3) = (-1, 0)$, while the ith hypermultiplet consists of two bifundamental chiral multiplets $Q_i, \tilde{Q}_i$ with $(r, I_3) = (0, 1/2)$. Here I_3 is a Cartan generator of $\mathrm{SU}(2)_I$. The pair $(Q_i, \tilde{Q}_i^\dagger)$ transforms in the doublet of $\mathrm{SU}(2)_I$ and have $\mathrm{U}(1)_i$ charge $F_i = -1$. From the view point of $\mathcal{N} = 1$ supersymmetry, the $\mathrm{U}(1)$ symmetry generated by the combination

$$\mathcal{F} = r + I_3 \tag{1.20}$$

is a flavor symmetry. We denote the fugacity for $\mathcal{F}$ by t. For the standard definition of the $\mathcal{N} = 2$ index, r and $\mathcal{F}$ enter the trace through the combination $(pq)^{-r} t^{\mathcal{F}}$. Then, the fugacities of $Q_i, \tilde{Q}_i$ and Φ_i are $\sqrt{t}/\alpha_i$, $\sqrt{t}\alpha_i$ and pq/t, respectively.

It is helpful for us to prepare two copies for each node of the quiver and impose identification between them. We draw the arrows in such a way that Φ_i connects the two copies of the ith node and makes a triangle with Q_i and $\tilde{Q}_i$, as in figure 8. Drawn in this form, it is clear that the $\mathcal{N} = 2$ linear quiver is a special case of the triangle quiver described in section 1.1, except that the vertical arrow is missing between the flavor nodes at the right end. The corresponding brane tiling diagram is therefore essentially the same, as shown in figure. Note that the cubic superpotentials, generated around the triangles by world-sheet instantons, are precisely what we need for the theory to have $\mathcal{N} = 2$ supersymmetry.

As we can split the $(m + 1)$-punctured sphere into a collection of m trinions, we can also break the brane tiling diagram into basic pieces. Each piece represents a single trinion and

is made of three zig-zag paths:

(1.21)

Gluing two trinions corresponds to concatenating two such diagrams side by side. In the course of this operation, we must interchange the positions of the zig-zag paths labeled b and c near the glued side of one of the diagrams. This results in an additional vertical arrow in the combined quiver, which is the adjoint chiral multiplet in the $\mathcal{N}=2$ vector multiplet used in the gauging.

Let us find the relationship between the convention we use for brane tilings and that used above. The R-charge R in the brane tiling model is given in terms of the charges of the $\mathcal{N}=2$ theory by

$$R = R_0 + \frac{1}{2}\sum_i F_i, \quad R_0 = -r + I_3.$$

(1.22)

The flavor charges associated to the zig-zag paths can be written as

$$F_{a_i} = -F_i, \quad F_b = -\mathcal{F} + \frac{1}{2}\sum_i F_i, \quad F_c = \mathcal{F} + \frac{1}{2}\sum_i F_i.$$

(1.23)

Without loss of generality, we can set

$$a_i = \frac{1}{\alpha_i}.$$

(1.24)

Plugging these relations into the combination $(pq)^{R/2}\prod_i a_i^{F_{a_i}} b^{F_b} c^{F_c}$ that enters the indices of the bifundamental chiral multiplets, we deduce

$$b = \frac{1}{\sqrt{t}}, \quad c = \sqrt{\frac{t}{pq}}.$$

(1.25)

Before proceeding, we should mention a peculiarity in the A_1 case. When $N=2$, the U(1) flavor symmetry of a bifundamental hypermultiplet is enhanced to SU(2) due to the fact that the fundamental representation of SU(2) is pseudoreal. For this reason there is no distinction between minimal and maximal punctures, and each trinion can be regarded as a half-hypermultiplet in the trifundamental representation of SU(2)^3. This is reflected in the index of a trinion,

$$\mathcal{I}_B(w, z; \sqrt{t}a)\mathcal{I}_B(z, w; \sqrt{t}/a) = \Gamma(\sqrt{t}a^{\pm 1}z^{\pm 1}w^{\pm 1}),$$

(1.26)

which is manifestly symmetric under permutation of a, z and w.

1.3 Surface defects as transfer matrices

We are now ready to check the correspondence between surface defects and transfer matrices by comparing them with independent calculations. In this section we perform the simplest such check for surface defects in A_1 theories of class-$\mathcal{S}$, which arise from compactification of the six-dimensional $\mathcal{N} = (2,0)$ theory of type A_1 on punctured Riemann surfaces. We see that for the case of the fundamental representation of SU(2), the surface defect is locally identified with the L-operator of Derkachov and Spiridonov [30].

1.3.1 Surface defects and L-operators

Now we introduce a half-BPS surface defect, and put it on $S^1 \times S^1 \subset S^1 \times S^3$. The second S^1 factor may be taken to be either $\{\zeta_1 = 0\}$ or $\{\zeta_2 = 0\}$ in the parametrization $|\zeta_1|^2 + |\zeta_2|^2 = 1$ of S^3. These are the circles in S^3 that are left invariant under the action of the isometry group $\mathrm{U}(1)_p \times \mathrm{U}(1)_q$. As explained in section **??**, the index in the presence of the surface defect is again given by a correlation function of line operators in a 2d TQFT on Σ. The correlator now contains a new line operator created by the D3-brane ending on the D5-branes, which was denoted by dashed line:

$$\text{-------->} \quad . \tag{1.27}$$

This line operator is specified by a representation of SU(N) [31–33]. In fact, it is labeled with a pair of representations (R_1, R_2) since in general we can take superposition of two surface defects, each wrapped around either circle in S^3.

In any case, the correlation function equals the partition function of a lattice model whose lattice is made of two kinds of lines, zig-zag paths coming from NS5-branes and the dashed line coming from the D3-branes. An extra dimension emerges as the M-theory circle if the brane system is embedded in the M-theory via T-duality along the first S^1 factor. Under this embedding, the D3-branes are mapped to M2-branes supported at points on the M-theory circle. Thus, the inclusion of the dashed line does not spoil the integrability of the lattice model. Moreover, by deforming the zig-zag paths near the dashed line, we can always make the neighborhood of the dashed line look like

$$\overset{\displaystyle \quad\uparrow\qquad\uparrow\qquad\qquad\uparrow}{\subset \!\!\rightarrow\!\! \text{---} \cdots \text{---} \!\! \supset} \tag{1.28}$$
$$\quad 1 \quad\; 2 \qquad\qquad n$$

in some (N, q) 5-brane background. Each crossing of a solid line and the dashed one gives us an R-operator, which we call L-operator. Thus we conclude that the surface defect is represented in the lattice model by the insertion of a transfer matrix constructed from L-operators.

If a dashed line is in an k-dimensional representation, the L-operator in an $(N, -1)$ background

$$L = \quad \text{◼} \quad = \quad \text{◼} \tag{1.29}$$

14

may be represented as an $k \times k$ matrix, whose entries are difference operators acting on the fugacities for the flavor node associated with the $(N, 0)$ region below the dashed line. It satisfies the RLL relation with the R-matrix (1.6); which we denote by $R^\diamond$. This R-matrix defines the Bazhanov-Sergeev model of type $SU(N)$ [6, 34, 35].

In what follows, we first compute the L-operator in lattice model side. Then proceed to the independent calculation of surface defects in gauge theory side.

1.3.2 Fundamental representation of $SU(2)$

Let us consider the simplest interesting setup where we have just two D5-branes and a single D3-brane, and identify the concrete form of the transfer matrix (1.28) in this case. For $N = 2$, (N, q) and $(N, q + 2)$ 5-branes are related by an $SL(2; \mathbb{Z})$ transformation of type IIB string theory. Therefore, we can go to a duality frame in which the transfer matrix only involves either $(N, 0)$ or $(N, -1)$ regions or $(N, 0)$ or $(N, 1)$ regions. The two cases are on an equal footing, and in fact related in a simple way. So we focus on the transfer matrix in the $(N, -1)$ background.

We denote the L-operator in this case by $L^\diamond$ since it is the operator that arises when a dashed line is inserted in a brane tiling model described by the diamond quiver constructed from the R-operator (1.6). In the situation under consideration, the gauge group of a brane tiling model is a product of $SU(2)$ groups, and the surface defect is labeled by $(R_1, R_2) = (\emptyset, \square)$; the D3-brane wraps the circle $\{\zeta_2 = 0\}$ in S^3. Let $V^\diamond$ be the space of meromorphic functions $f(z)$ such that $f(z) = f(1/z)$, and $W = \mathbb{C}^2$. Then we can represent $L^\diamond : W \otimes V^\diamond \to V^\diamond \otimes W$ as a 2×2 matrix whose entries are operators acting on functions in $V^\diamond$. The R-matrix $\mathcal{R}_{ij}^\diamond : W_i \otimes W_j \to W_j \otimes W_i$ is just a 4×4 matrix. (Here all the W_i are $\mathbb{C}^2$.) These operators, together with the R-operator $R^\diamond$ of Bazhanov-Sergeev type, satisfy the Yang-Baxter equations and RLL relations.

On the other hand, in the context of integrable lattice models Sklyanin constructed an L-operator $L^S : W \otimes V^\diamond \to V^\diamond \otimes W$ that solves the RLL relation [36]

$$\mathcal{R}_{12}^B(u_1, u_2) L_1^S(u_1, (\nu, l)) L_2^S(u_2, (\nu, l)) = L_2^S(u_2, (\nu, l)) L_1^S(u_1, (\nu, l)) \mathcal{R}_{12}^B(u_1, u_2), \qquad (1.30)$$

with Baxter's R-matrix $\mathcal{R}_{ij}^B : W_i \otimes W_j \to W_j \otimes W_i$ for the eight-vertex model [37, 38]. Here u_i is a complex spectral parameter for W_i, and (ν, l) is a pair of complex spectral parameters for $V^\diamond$. Baxter's R-matrix solves the Yang-Baxter equation

$$\mathcal{R}_{12}^B(u_1, u_2) \mathcal{R}_{13}^B(u_1, u_3) \mathcal{R}_{23}^B(u_2, u_3) = \mathcal{R}_{23}^B(u_2, u_3) \mathcal{R}_{13}^B(u_1, u_3) \mathcal{R}_{12}^B(u_1, u_2), \qquad (1.31)$$

and the solution is given by

$$\mathcal{R}_{ij}^B(u_i, u_j) = P \sum_{a=0}^{3} w_a(u_i - u_j) \sigma_a \otimes \sigma_a, \quad w_a(u) = \frac{\theta_{a+1}(u + \eta)}{\theta_{a+1}(\eta)}, \qquad (1.32)$$

where $P : W_i \otimes W_j \to W_j \otimes W_i$ is the permutation operator, σ_a are the Pauli matrices and 2×2 unit matrix, $\theta_{a+1}(u) = \theta_{a+1}(u|\tau)$ are the Jacobi theta functions, and τ, η are complex

15

parameters of the eight-vertex model. Sklyanin's L-operator is defined by

$$L^{\mathrm{S}}(u,(\nu,l)) = P \sum_{a=0}^{3} w_a(u+\eta)\sigma_a \otimes \mathbf{S}_a^{(l)}. \tag{1.33}$$

The operators $\mathbf{S}_a^{(l)}$ act on meromorphic functions $f(\zeta)$ as difference operators:

$$\left(\mathbf{S}_a^{(l)} f\right)(\zeta) = \mathrm{i}^{\delta_{a,0}} \frac{\theta_{a+1}(\eta)}{\theta_{a+1}(2\zeta)} \left(\theta_{a+1}(2\zeta - 2\eta l)f(\zeta+\eta) - \theta_{a+1}(-2\zeta - 2\eta l)f(\zeta-\eta)\right). \tag{1.34}$$

They generate the so-called Sklyanin algebra [39].

In [30], Derkachov and Spiridonov constructed an R-operator $R_{ij}^{\mathrm{DS}} : V_i^{\diamond} \otimes V_j^{\diamond} \to V_j^{\diamond} \otimes V_i^{\diamond}$ that satisfies the RLL relation

$$R_{12}^{\mathrm{DS}}((\nu_1,l_1),(\nu_2,l_2))L_2^{\mathrm{DS}}(u,(\nu_2,l_2))L_1^{\mathrm{DS}}(u,(\nu_1,l_1))$$
$$= L_1^{\mathrm{DS}}(u,(\nu_1,l_1))L_2^{\mathrm{DS}}(u,(\nu_2,l_2))R_{12}^{\mathrm{DS}}((\nu_1,l_1),(\nu_2,l_2)), \tag{1.35}$$

The L-operator $L^{\mathrm{DS}} : W \otimes V^{\diamond} \to V^{\diamond} \otimes W$ is essentially Sklyanin's L-operator, differing only by an automorphism of the Sklyanin algebra:

$$L^{\mathrm{DS}}(u,(\nu,l)) = \varphi\sigma_3 L^{\mathrm{S}}\varphi^{-1}, \quad (\varphi f)(\zeta) := \exp(\pi \mathrm{i}\zeta^2/\eta)f(\zeta). \tag{1.36}$$

This L-operator again satisfies the RLL relation with Baxter's R-matrix $\mathcal{R}^{\mathrm{B}}$. At this point, what is important is that Derkachov and Spiridonov show their R-operator R^{DS} is precisely the R-operator for the diamond quiver in the brane tiling model $R^{\diamond}$, that is,

$$R_{ij}^{\mathrm{DS}}((\nu_i,l_i),(\nu_j,l_j)) = R_{ij}^{\diamond}((a_i,b_i),(a_j,b_j)), \tag{1.37}$$

with the variables ζ and z are related by $z = \exp(2\pi \mathrm{i}\zeta)$ and the parameters identified as

$$a_i b_i = \exp(-2\pi \mathrm{i}\nu_i), \quad \frac{a_i}{b_i} = \exp(2\pi \mathrm{i}\eta(2l_i + 1)), \tag{1.38}$$

$$(p,q) = (\exp(2\pi \mathrm{i}\tau), \exp(4\pi \mathrm{i}\eta)). \tag{1.39}$$

Based on these observations, a natural counterpart of the L-operator for the diamond quiver

$$L^{\diamond}(c,(a,b)) = \quad c \text{-----} \rightarrow \tag{1.40}$$
$$(a,b)$$

is the L-operator of Derkachov and Spiridonov:

$$L^{\mathrm{DS}}(u,(\nu,l)) = L^{\diamond}(c,(a,b)). \tag{1.41}$$

Requiring $L^{\diamond}(c,(a,b)) = L^{\diamond}(1,(a/c,b/c))$ fixes the relation between the two spectral parameters for the dashed line to be

$$c = \exp(\pi \mathrm{i}u). \tag{1.42}$$

For the computation of the transfer matrix, we exploit the fact that $L^\diamond$ really consists of three parts separated by zig-zag paths:

$$L_i^\diamond(c,(a_i,b_i)) = \quad c \quad \begin{array}{c} b_i \\ \boxed{\;\;z_i\;\;} \\ a_i \end{array} \quad . \tag{1.43}$$

Reflecting this structure, $L^\diamond$ can be expressed in the following factorized form:

$$L_i^\diamond(c,(a_i,b_i)) = B\left(z_i;\frac{b_i}{c}\right) \cdot \varphi(z_i)\frac{1}{\theta_1(z_i^2)} \begin{pmatrix} \Delta_i^{1/2} & 0 \\ 0 & \Delta_i^{-1/2} \end{pmatrix} \varphi^{-1}(z_i) \cdot A\left(z_i;\frac{a_i}{c}\right). \tag{1.44}$$

In this expression, $\Delta_i^{\pm 1/2}$ are difference operators acting on functions of z_i as $\left(\Delta_i^{\pm 1/2}f\right)(z_i) = f(q^{\pm 1/2}z_i)$ and

$$A(z;a) = \begin{pmatrix} \bar\theta_4(a/z) & \bar\theta_3(a/z) \\ \bar\theta_4(az) & \bar\theta_3(az) \end{pmatrix}, \quad B(z;b) = \begin{pmatrix} \bar\theta_3(bz) & -\bar\theta_3(b/z) \\ \bar\theta_4(bz) & -\bar\theta_4(b/z) \end{pmatrix}, \tag{1.45}$$

where $\bar\theta_a(z) = \theta_a(z;\sqrt{p})$ and we used the multiplicative notation for the theta functions. Roughly speaking, one can think of the three matrices in the expression (1.44) as corresponding to the left, middle and right parts of the above diagram.

The transfer matrix (1.28) is obtained by concatenating n copies of the pieces (1.43) along a loop:

$$c \quad \begin{array}{cccc} b_1 & b_2 & & b_n \\ \boxed{\;z_1\;} & \boxed{\;z_2\;} & \cdots & \boxed{\;z_n\;} \\ a_1 & a_2 & & a_n \end{array} \quad . \tag{1.46}$$

Thus, multiplying n copies of the L-operators (1.44) and using formulas in the appendix, we obtain the following formula for the transfer matrix:

$$\mathrm{Tr}_W\left(L_n^\diamond(c,(a_n,b_n)) \circ_W \cdots \circ_W L_1^\diamond(c,(a_1,b_1))\right)$$

$$= \sum_{s_1=\pm 1} \cdots \sum_{s_n=\pm 1} \prod_{i=1}^n \ell\left(z_{i-1}^{s_{i-1}}, z_i^{s_i}; \frac{b_{i-1}}{c}, \frac{a_i}{c}\right) \prod_{j=1}^n \Delta_j^{s_j/2}, \tag{1.47}$$

where

$$\ell(w,z;b,a) = \frac{1}{\theta(z^2)}\theta\left(\sqrt{\frac{p}{q}}ba\frac{w}{z}\right)\theta\left(\sqrt{\frac{p}{q}}\frac{a}{b}\frac{1}{wz}\right). \tag{1.48}$$

In this formula we have dropped off an overall constant independent of the spectral parameters. At any rate, the overall normalization of the L-operators is irrelevant and cannot be determined by the RLL relations. The RLL relations actually admit more degrees of freedom than just the overall normalization. For example, we can multiply $L^\diamond(c,(a,b))$ by a function $f(c,(a,b))$ of its spectral parameters, and the new one still solves the RLL relations.

17

In section 1.3.4 we will check the correspondence by comparing (1.47) with independent computations in gauge theory.

So far we have considered the surface defect labeled as $(R_1, R_2) = (\emptyset, \square)$. Of course, we may also consider the case with $(R_1, R_2) = (\square, \emptyset)$ in the same manner, by letting surface defects wrap around the other S^1 inside S^3. Hence, there are two sets of L-operators related by the symmetry exchanging p and q. The underlying algebraic structure is the product of two copies of the Sklyanin algebra, known as the *elliptic modular double* [40]. Also, with the knowledge of the transfer matrix in the $(N, -1)$ 5-brane background, we can obtain the transfer matrix in the $(N, 1)$ background by taking a conjugation with a loop of bifundamental chiral multiplet. This relation is actually the consequence of the Yang-Baxter equation. For more details and other aspects, see [1].

1.3.3 Surface defects in A_1 theories of class-$\mathcal{S}$

Let us proceed to the independent computation in gauge theory side. The action of surface defects on the supersymmetric indices of class-$\mathcal{S}$ theories have been studied in [33, 41–43]. In [41], it was explained how to construct a surface defect labeled with a pair of integers (r, s), and how to determine its action on the supersymmetric index. Although the method applies to general $\mathcal{N} = 2$ theories with $\mathrm{SU}(N)$ flavor symmetry, here we review it in the language of class-$\mathcal{S}$ theories.

Suppose we have a class-$\mathcal{S}$ theory $\mathcal{T}_{\mathrm{IR}}$ associated to a Riemann surface that contains a maximal puncture, whose flavor group we call $\mathrm{SU}(N)_z$. To this surface we introduce an extra minimal puncture. Concretely, we can do this as follows. First, we rename the flavor group $\mathrm{SU}(N)_z$ to $\mathrm{SU}(N)_{w'}$. Then, we take trinion representing a hypermultiplet $(Q, \tilde{Q})$ with flavor symmetry $\mathrm{SU}(N)_{w''} \times \mathrm{SU}(N)_z \times \mathrm{U}(1)_\alpha$, and glue it to $\mathcal{T}_{\mathrm{IR}}$ by gauging the diagonal subgroup $\mathrm{SU}(N)_w$ of $\mathrm{SU}(N)_{w'} \times \mathrm{SU}(N)_{w''}$. The resulting theory $\mathcal{T}_{\mathrm{UV}}$ has one more flavor symmetry, $\mathrm{U}(1)_\alpha$, than $\mathcal{T}_{\mathrm{IR}}$. Correspondingly, the surface associated to $\mathcal{T}_{\mathrm{UV}}$ has one more minimal puncture than the original surface.

The theory $\mathcal{T}_{\mathrm{UV}}$ is related to $\mathcal{T}_{\mathrm{IR}}$ via the RG flow induced by a diagonal constant vev given to the quark Q, or equivalently, to the baryon $B = \det Q$. The vev higgses the gauge group $\mathrm{SU}(N)_w$ and breaks $\mathrm{SU}(N)_w \times \mathrm{SU}(N)_z$ down to the diagonal subgroup. Moreover, it turns the cubic superpotential $\tilde{Q}\Phi Q$ into a quadratic one that makes $\tilde{Q}$ and Φ massive, where Φ is the adjoint chiral multiplet introduced in the gluing. Up to Nambu-Goldstone multiplets that survive the higgsing, in the infrared the multiplets we added are gone and we recover $\mathcal{T}_{\mathrm{IR}}$, with $\mathrm{SU}(N)_w$ replaced with $\mathrm{SU}(N)_z$. In effect, the minimal puncture introduced by gluing the trinion is "closed." The R-charge I_3 is broken by the vev, but the combination $I_3 + F_\alpha/2$ is preserved and identified with a Cartan generator of the infrared $\mathrm{SU}(2)$ R-symmetry.

To create a surface defect in $\mathcal{T}_{\mathrm{IR}}$, we instead give the baryon a position-dependent vev $\langle B \rangle = \zeta_1^r \zeta_2^s$. Here, as before, ζ_1 and ζ_2 are complex coordinates of the two orthogonal planes rotated by $j_p = j_1 + j_2$ and $j_q = j_1 - j_2$, respectively. Away from the origin, the effect of the position-dependent vev is the same as that of the constant vev, so we get $\mathcal{T}_{\mathrm{IR}}$ in the

infrared. If $r \neq 0$, however, the infrared theory is modified on the plane $\{\zeta_1 = 0\}$ since the vev vanishes there. By the same token, the theory is modified on the plane $\{\zeta_2 = 0\}$ if $s \neq 0$. Hence, in general we obtain $\mathcal{T}_{\mathrm{IR}}$ with the insertion of a surface defect labeled with the pair of integers (r, s), supported on the planes $\{\zeta_1 = 0\}$ and $\{\zeta_2 = 0\}$. This surface defect is to be identified with the surface defect labeled with the pair

$$(\underbrace{\square\square\cdots\square}_{r}, \underbrace{\square\square\cdots\square}_{s})$$

of symmetric representation of $\mathrm{SU}(N)$ discussed in the previous subsection [33].

The index of $\mathcal{T}_{\mathrm{UV}}$ has a pole in the α-plane at $\alpha = \sqrt{t}p^{r/N}q^{s/N}$, and the residue there gives the index of $\mathcal{T}_{\mathrm{IR}}$ in the presence of the surface defect of type (r, s). The reason is the following. The position-dependent vev $\langle B \rangle = \zeta_1^r \zeta_2^s$ breaks $\mathrm{U}(1)_p$, $\mathrm{U}(1)_q$, and $\mathrm{SU}(2)_I$. At this value of α, however, the only combinations of charges that enter the trace defining the index are those that are preserved by the vev. Thus, we can still define the index in this background. As explained above, $\mathcal{T}_{\mathrm{UV}}$ flows to $\mathcal{T}_{\mathrm{IR}}$ plus Nambu-Goldstone multiplets in the infrared. The latter contains massless degrees of freedom, and they contribute to the index by a diverging factor, in fact a simple pole in the α-plane. Therefore, the residue at this pole gives the index of $\mathcal{T}_{\mathrm{IR}}$, together with some factor associated with the Nambu-Goldstone multiplets.

We wish to compute this residue and determine the action of the surface defect on the index in the simplest non-trivial case, namely when $N = 2$ and $(r, s) = (0, 1)$. But first, let us look at the trivial case $(r, s) = (0, 0)$ to gain intuition of the computation.

In the construction of a surface defect described above, $\tilde{Q}$ and Φ actually play no role. The essential point is that the vev given to the baryon built from Q replaces $\mathrm{SU}(N)_w$ with $\mathrm{SU}(N)_z$ in the infrared. So we couple $\mathcal{T}_{\mathrm{IR}}$ just to Q for the moment. The index of the combined theory is given by

$$\int_{\mathbb{T}} \frac{dw}{2\pi i w} \mathcal{I}_{\mathrm{V}}(w) \mathcal{I}_{\mathrm{B}}(z, w; \rho) \mathcal{I}_{\mathcal{T}_{\mathrm{IR}}}(w) = \kappa \int_{\mathbb{T}} \frac{dw}{2\pi i w} \frac{\Gamma(\rho z^{\pm 1} w^{\pm 1})}{\Gamma(w^{\pm 2})} \mathcal{I}_{\mathcal{T}_{\mathrm{IR}}}(w), \qquad (1.49)$$

where $\rho = \sqrt{t}/a$ is the fugacity of Q and $\kappa = (p; p)_\infty (q; q)_\infty / 2$. In this integral, $|\rho| < 1$ is assumed, but we can analytically continue ρ to a complex parameter and study its pole structure. At $\rho = 1$, a constant vev be turned on for B without conflicting with the definition of the index. The integral should have a pole at this point in the p-plane, and we want to calculate the residue there.

The integrand has two pairs of poles in the w-plane at

$$w = \rho z, \, \rho^{-1} z; \qquad w = \rho z^{-1}, \, \rho^{-1} z^{-1}. \qquad (1.50)$$

As $\rho \to 1$, the first pair of poles collide and pinch the integration contour, and the integral diverges. Likewise, the second pair also collide in this limit. The pole of the integral in the ρ-plane arises from the contributions from these poles in w. Using formula (??), we find that

the contribution from the pole at $w = \rho z$ is

$$\frac{1}{2} \frac{\Gamma(\rho^2 z^2)\Gamma(z^{-2})}{\Gamma(\rho^2 z^2)\Gamma(\rho^{-2} z^{-2})} \Gamma(\rho^2) \mathcal{I}_{\mathcal{T}_{\mathrm{IR}}}(\rho z). \tag{1.51}$$

The last factor $\Gamma(\rho^2)$ indeed has a pole at $\rho = 1$, with residue $1/4\kappa$. The pole at $w = \rho z^{-1}$ makes an equal contribution, and we get

$$\mathrm{Res}_{\rho=1} \left[\int_{\mathbb{T}} \frac{dw}{2\pi i w} \mathcal{I}_{\mathrm{V}}(w) \mathcal{I}_{\mathrm{B}}(z, w; \rho) \mathcal{I}_{\mathcal{T}_{\mathrm{IR}}}(w) \right] = \frac{1}{2} \frac{1}{2\kappa} \mathcal{I}_{\mathcal{T}_{\mathrm{IR}}}(z). \tag{1.52}$$

As expected, the residue reproduces the index of $\mathcal{T}_{\mathrm{IR}}$, multiplied by some factors. The factor of $1/2$ comes from the fact that B has fugacity ρ^2, and disappears if we add the equal contribution from the pole at $\rho = -1$. The factor $1/2\kappa$ is the contribution from a decoupled free chiral multiplet contained in a Nambu-Goldstone multiplet. It is the inverse of the index of a free vector multiplet since higgsing of a U(1) gauge theory with a single chiral multiplet leads to a trivial theory whose index is one.

In order to express this result in a concise form, we introduce the notation of "striking out an arrow" in a quiver diagram to indicate that a constant vev is given to the baryonic operator built from the bifundamental chiral multiplet represented by that arrow, and the notation, what we just found is the identity

$$\boxed{z} \xrightarrow{\rho}\!\!\!\!\!/\; \text{\textcircled{w}} \;= 4\kappa \mathrm{Res}_{\rho=1} \left[\boxed{z} \xrightarrow{\rho} \text{\textcircled{w}} \right] = \boxed{z} =\!\!\!= \text{\textcircled{w}} \quad, \tag{1.53}$$

where the right-hand side is the delta function defined by the relation (1.17). This identity holds when the index of any theory with SU(2) flavor symmetry (or more generally, any meromorphic function $f(w)$ such that $f(w) = f(1/w)$) is coupled to the right node.

With the help of this identity, we can readily show that when a constant vev is turned on for B, the index of $\mathcal{T}_{\mathrm{UV}}$ reduces to that of $\mathcal{T}_{\mathrm{IR}}$. All we have to do is to look at the part of $\mathcal{T}_{\mathrm{UV}}$ describing the coupling to the trinion, and compute the relevant residue:

$$\tag{1.54}$$

In the first equality we use the identity (1.53) and set $\rho = 1$, and in the second we canceled the pair of arrows making a loop. Thus, the vev transforms the trinion into the original flavor node of $\mathcal{T}_{\mathrm{IR}}$.

We can compute the index of $\mathcal{T}_{\mathrm{IR}}$ in the presence of a surface defect in a similar manner. To indicate that the position-dependent vev $\langle B \rangle = \zeta_1^r \zeta_2^s$ is turned on, we put the label (r, s) on the struck-out arrow:

$$\boxed{z} \xrightarrow[\;(r,s)\;]{\rho}\!\!\!\!\!/\; \text{\textcircled{w}} \;= 4\kappa \mathrm{Res}_{\rho=p^{-r/2} q^{-s/2}} \left[\boxed{z} \xrightarrow{\rho} \text{\textcircled{w}} \right] \quad. \tag{1.55}$$

Then the action of the surface defect of type (r, s) on the index is encoded in the diagram

$$
\begin{array}{c}
\text{\large w} \longrightarrow \boxed{z} \\
\Big\downarrow \diagdown \\
\text{\large w} \quad {\scriptstyle (r,s)}
\end{array}
\qquad .
\tag{1.56}
$$

Let us calculate the residue (1.56) for $(r, s) = (0, 1)$. At $\rho = q^{-1/2}$, the index $\mathcal{I}_B(z, w; \rho) = \Gamma(\rho z^{\pm 1} w^{\pm 1})$ of Q has four sets of colliding poles in the w-plane. Two of them are

$$
w = \rho q z, \ \rho^{-1} z; \qquad w = \rho z^{-1}, \ \rho^{-1} q^{-1} z^{-1},
\tag{1.57}
$$

while the other two are

$$
w = \rho q z^{-1}, \ \rho^{-1} z^{-1}; \qquad w = \rho z, \ \rho^{-1} q^{-1} z.
\tag{1.58}
$$

The contributions to the residue come from these poles. A small calculation shows that the first two sets of poles contribute in the same way: they set $w = q^{1/2} z$ and give a factor of $1/\theta(q^{-1})\theta(z^2)$ in total. Similarly, the contributions from the last two set $w = q^{-1/2} z$ and give a factor of $1/\theta(q^{-1})\theta(z^{-2})$. Altogether, we find that the result can be expressed as

$$
\boxed{z} \xrightarrow[(0,1)]{\ \rho\ } \text{\large w} \ = \ \frac{1}{\theta(q^{-1})} \sum_{s=\pm 1} \frac{1}{\theta(z^{2s})} \Delta^{s/2} \boxed{z} =\!\!= \text{\large w}
\tag{1.59}
$$

We remind the reader that $\theta(z) = \theta(z; p)$ and $\Delta^{\pm 1/2}$ act on functions of z as $\left(\Delta^{\pm 1/2} f\right)(z) = f(q^{\pm 1/2} z)$.

Unlike the case of the constant vev, this identity does not cause a complete cancelation of the indices of $\tilde{Q}$ and Φ. Rather, for $\rho = q^{-1/2}$ and $w = q^{\pm 1/2} z$, we have

$$
\begin{array}{c}
\boxed{w} \xrightarrow{\ \sqrt{t}\alpha\ } \boxed{z} \\
{\scriptstyle pq/t} \Big\uparrow \\
\boxed{w}
\end{array}
\ = \ \theta\left(\frac{t}{q} z^{\mp 2}\right) \theta(t).
\tag{1.60}
$$

Therefore, the effect of introducing the surface defect of type $(0, 1)$ on the index is realized by the difference operator

$$
\mathfrak{S}_{(0,1)} = \frac{\theta(t)}{\theta(q^{-1})} \sum_{s=\pm 1} \frac{1}{\theta(z^{2s})} \theta\left(\frac{t}{q} z^{-2}\right) \Delta^{s/2}.
\tag{1.61}
$$

The prefactor $\theta(t)/\theta(q^{-1})$ is equal to the index of a free chiral field in two dimensions, and represents the center-of-mass degree of freedom of the surface defect.

The difference operator $\mathfrak{S}_{(0,1)}$ acts on the fugacity for the maximal puncture on which the surface defect was constructed. This fact has a natural interpretation. To construct the surface defect, we first introduced an extra minimal puncture, and then took the residue of a pole in the fugacity of the associated flavor symmetry. The latter step can be thought of as transforming the minimal puncture to another kind of puncture which represents the
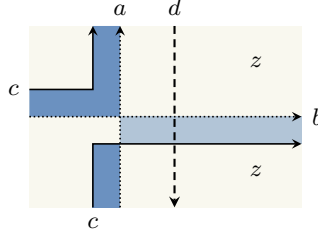
Figure 9: The brane tiling representation of a surface defect acting on a maximal puncture.

surface defect. By construction, this puncture is located in the neighborhood of a maximal puncture contained in a trinion. We can take the surface defect puncture and collide it to the maximal puncture. The collision produces a new puncture, and defines the action of the surface defect on the maximal puncture.

1.3.4 Comparison with the transfer matrix

Let us finally compare the result with the proposal. For clarity of presentation, take a minimal puncture in $\mathcal{T}_{\mathrm{IR}}$ and move it close to the maximal puncture on which the surface defect acts. Then the neighborhood of these punctures looks like a trinion glued to another maximal puncture, and is represented by zig-zag paths as in figure 9.

According to the general argument, the surface defect creates a dashed line with some spectral parameter d, drawn in the picture as well. It acts on the lattice model as the transfer matrix (1.47), constructed from a single L-operator

$$\mathrm{Tr}\left(L^{\diamond}(d,(c,b))\right) = \sum_{s=\pm 1} \frac{1}{\theta(z^{2s})}\theta\left(\sqrt{\frac{p}{q}}\frac{bc}{d^2}\right)\theta\left(\sqrt{\frac{p}{q}}\frac{c}{b}z^{-2s}\right)\Delta^{s/2}. \tag{1.62}$$

From the relation (1.25), we see that if we set

$$d = \frac{1}{\sqrt{qt}}, \tag{1.63}$$

the transfer matrix indeed reproduces the difference operator (1.61), up to an overall factor which cannot be fixed by the Yang-Baxter equations. As noted in [41], the above transfer matrix is essentially the Hamiltonian of elliptic Ruijsenaars-Schneider model [44, 45] of type A_1. This fact follows from a general result obtained in [46].

Here we have considered only the surface defect of type $(0,1)$, but the general story is similar. The surface defect of type (r,s) acts on the index by a difference operator $\mathfrak{S}_{(r,s)}$. This operator is expected to coincide with the transfer matrix for an appropriate L-operator. If so, by the RLL relation, the operators $\mathfrak{S}_{(r,s)}$ for all (r,s) should commute with each other. This is indeed true [41]. From the class-$\mathcal{S}$ point of view, the mutual commutativity is guaranteed by the fact that the index is independent of the positions of punctures representing surface defects. Therefore, the order in which they act on a maximal puncture is irrelevant. Note that this argument also exploits the existence of an extra dimension, which is the M-theory

circle that emerges as the type IIA brane configuration is lifted to M-theory. For the same reason, a surface defect puncture can be placed between any two punctures, whether minimal or maximal, and still yield the same result. From the point of view of the type IIA system, this property appears to be quite non-trivial and is known as the "hopping invariance" of the index [33]. From the lattice model viewpoint, this is guaranteed by the other kind of RLL relation.

For the fundamental representation of SU(2), the above L-operator is essentially identified with Sklyanin's L-operator, which satisfies the RLL relation with Baxter's R-matrix for the eight-vertex model and generates the so-called Sklyanin algebra. For the fundamental representation of SU(N) with general N, we get the L-operator for Belavin's elliptic R-matrix [47]. If instead placed in an $(N, 0)$ background, the L-operator gives a representation of Felder's elliptic quantum group for $\mathfrak{sl}_N$ [48–50]. Thus, the surface defects for general N unify these integrable lattice models and generate the so-called *elliptic quantum group*. For the details, see [51].

References

[1] K. Maruyoshi and J. Yagi, *Surface defects as transfer matrices*, *PTEP* **2016** (2016) 113B01, [`1606.01041`].

[2] A. Hanany and K. D. Kennaway, *Dimer models and toric diagrams*, `hep-th/0503149`.

[3] S. Franco, A. Hanany, K. D. Kennaway, D. Vegh and B. Wecht, *Brane dimers and quiver gauge theories*, *JHEP* **01** (2006) 096, [`hep-th/0504110`].

[4] K. D. Kennaway, *Brane Tilings*, *Int. J. Mod. Phys. A* **22** (2007) 2977–3038, [`0706.1660`].

[5] M. Yamazaki, *Brane Tilings and Their Applications*, *Fortsch. Phys.* **56** (2008) 555–686, [`0803.4474`].

[6] M. Yamazaki, *Quivers, YBE and 3-manifolds*, *JHEP* **05** (2012) 147, [`1203.5784`].

[7] M. Yamazaki, *New Integrable Models from the Gauge/YBE Correspondence*, *J. Statist. Phys.* **154** (2014) 895, [`1307.1128`].

[8] N. Seiberg, *Exact results on the space of vacua of four-dimensional SUSY gauge theories*, *Phys. Rev. D* **49** (1994) 6857–6863, [`hep-th/9402044`].

[9] N. Seiberg, *Electric - magnetic duality in supersymmetric nonAbelian gauge theories*, *Nucl. Phys. B* **435** (1995) 129–146, [`hep-th/9411149`].

[10] A. Hanany and D. Vegh, *Quivers, tilings, branes and rhombi*, *JHEP* **10** (2007) 029, [`hep-th/0511063`].

[11] C. Romelsberger, *Counting chiral primaries in N = 1, d=4 superconformal field theories*, *Nucl. Phys. B* **747** (2006) 329–353, [`hep-th/0510060`].

[12] J. Kinney, J. M. Maldacena, S. Minwalla and S. Raju, *An Index for 4 dimensional super conformal theories*, *Commun. Math. Phys.* **275** (2007) 209–254, [`hep-th/0510251`].

[13] G. Festuccia and N. Seiberg, *Rigid Supersymmetric Theories in Curved Superspace*, *JHEP* **06** (2011) 114, [`1105.0689`].

[14] V. Spiridonov and G. Vartanov, *Vanishing superconformal indices and the chiral symmetry breaking*, *JHEP* **06** (2014) 062, [`1402.2312`].

[15] V. P. Spiridonov, *Theta hypergeometric integrals*, *Algebra i Analiz* **15** (2003) 161–215.

[16] E. M. Rains, *Transformations of elliptic hypergeometric integrals*, *Ann. of Math. (2)* **171** (2010) 169–243.

[17] F. Dolan and H. Osborn, *Applications of the Superconformal Index for Protected Operators and q-Hypergeometric Identities to N=1 Dual Theories*, *Nucl. Phys. B* **818** (2009) 137–178, [0801.4947].

[18] J. Yagi, *Quiver gauge theories and integrable lattice models*, *JHEP* **10** (2015) 065, [1504.04055].

[19] D. Gaiotto, $N = 2$ *dualities*, *JHEP* **08** (2012) 034, [0904.2715].

[20] D. Gaiotto, G. W. Moore and A. Neitzke, *Wall-crossing, Hitchin Systems, and the WKB Approximation*, 0907.3987.

[21] L. F. Alday, D. Gaiotto and Y. Tachikawa, *Liouville Correlation Functions from Four-dimensional Gauge Theories*, *Lett. Math. Phys.* **91** (2010) 167–197, [0906.3219].

[22] N. Wyllard, *A(N-1) conformal Toda field theory correlation functions from conformal* $\mathcal{N} = 2$ *SU(N) quiver gauge theories*, *JHEP* **11** (2009) 002, [0907.2189].

[23] A. Gadde, E. Pomoni, L. Rastelli and S. S. Razamat, *S-duality and 2d Topological QFT*, *JHEP* **03** (2010) 032, [0910.2225].

[24] A. Gadde, L. Rastelli, S. S. Razamat and W. Yan, *The 4d Superconformal Index from q-deformed 2d Yang-Mills*, *Phys. Rev. Lett.* **106** (2011) 241602, [1104.3850].

[25] T. Dimofte, D. Gaiotto and S. Gukov, *Gauge Theories Labelled by Three-Manifolds*, *Commun. Math. Phys.* **325** (2014) 367–419, [1108.4389].

[26] T. Dimofte, D. Gaiotto and S. Gukov, *3-Manifolds and 3d Indices*, *Adv. Theor. Math. Phys.* **17** (2013) 975–1076, [1112.5179].

[27] Y. Terashima and M. Yamazaki, *SL(2,R) Chern-Simons, Liouville, and Gauge Theory on Duality Walls*, *JHEP* **08** (2011) 135, [1103.5748].

[28] Y. Terashima and M. Yamazaki, *Emergent 3-manifolds from 4d Superconformal Indices*, *Phys. Rev. Lett.* **109** (2012) 091602, [1203.5792].

[29] J. Yagi, *3d TQFT from 6d SCFT*, *JHEP* **08** (2013) 017, [1305.0291].

[30] S. Derkachov and V. Spiridonov, *Yang-Baxter equation, parameter permutations, and the elliptic beta integral*, *Russ. Math. Surveys* **68** (2013) 1027–1072, [1205.3520].

[31] S. Gukov and E. Witten, *Gauge Theory, Ramification, And The Geometric Langlands Program*, hep-th/0612073.

[32] S. Gukov and E. Witten, *Rigid Surface Operators*, *Adv. Theor. Math. Phys.* **14** (2010) 87–178, [0804.1561].

[33] A. Gadde and S. Gukov, *2d Index and Surface operators*, *JHEP* **03** (2014) 080, [1305.0266].

[34] V. V. Bazhanov and S. M. Sergeev, *A Master solution of the quantum Yang-Baxter equation and classical discrete integrable equations*, *Adv. Theor. Math. Phys.* **16** (2012) 65–95, [1006.0651].

[35] V. V. Bazhanov and S. M. Sergeev, *Elliptic gamma-function and multi-spin solutions of the Yang-Baxter equation*, *Nucl. Phys. B* **856** (2012) 475–496, [1106.5874].

[36] E. K. Sklyanin, *Some algebraic structures connected with the Yang-Baxter equation*, *Funktsional. Anal. i Prilozhen.* **16** (1982) 27–34, 96.

[37] R. Baxter, *Eight-Vertex Model in Lattice Statistics*, *Phys. Rev. Lett.* **26** (1971) 832–833.

[38] R. J. Baxter, *Partition function of the eight vertex lattice model*, *Annals Phys.* **70** (1972) 193–228.

[39] E. K. Sklyanin, *Some algebraic structures connected with the Yang-Baxter equation. Representations of a quantum algebra*, *Funktsional. Anal. i Prilozhen.* **17** (1983) 34–48.

[40] V. P. Spiridonov, *The continuous biorthogonality of an elliptic hypergeometric function*, *Algebra i Analiz* **20** (2008) 155–185.

[41] D. Gaiotto, L. Rastelli and S. S. Razamat, *Bootstrapping the superconformal index with surface defects*, *JHEP* **01** (2013) 022, [1207.3577].

[42] L. F. Alday, M. Bullimore, M. Fluder and L. Hollands, *Surface defects, the superconformal index and q-deformed Yang-Mills*, *JHEP* **10** (2013) 018, [1303.4460].

[43] M. Bullimore, M. Fluder, L. Hollands and P. Richmond, *The superconformal index and an elliptic algebra of surface defects*, *JHEP* **10** (2014) 062, [1401.3379].

[44] S. N. M. Ruijsenaars and H. Schneider, *A new class of integrable systems and its relation to solitons*, *Ann. Physics* **170** (1986) 370–405.

[45] S. Ruijsenaars, *Complete Integrability of Relativistic Calogero-moser Systems and Elliptic Function Identities*, *Commun. Math. Phys.* **110** (1987) 191.

[46] K. Hasegawa, *Ruijsenaars' commuting difference operators as commuting transfer matrices*, *Comm. Math. Phys.* **187** (1997) 289–325.

[47] A. Belavin, *Dynamical Symmetry of Integrable Quantum Systems*, *Nucl. Phys. B* **180** (1981) 189–200.

[48] G. Felder, *Conformal field theory and integrable systems associated to elliptic curves*, hep-th/9407154.

[49] G. Felder, *Elliptic quantum groups*, in *11th International Conference on Mathematical Physics (ICMP-11) (Satellite colloquia: New Problems in the General Theory of Fields and Particles, Paris, France, 25-28 Jul 1994)*, pp. 211–218, 7, 1994, `hep-th/9412207`.

[50] G. Felder and A. Varchenko, *Elliptic quantum groups and Ruijsenaars models*, *J. Statist. Phys.* **89** (1997) 963–980.

[51] J. Yagi, *Surface defects and elliptic quantum groups*, *JHEP* **06** (2017) 013, [`1701.05562`].